Limits for interferometer calibration using the random ball test

Ping Zhou*, James H. Burge
College of Optical Science, Univ. of Arizona, 1630 E. Univ. Blvd, Tucson, AZ, USA 85721

ABSTRACT

The random ball test (RBT), also known as the CaliBall test, is often used to calibrate interferometer transmission spheres. This paper provides a way to estimate the total errors remaining after interferometer calibration using the RBT. Errors that cannot be removed by calibration include random errors due to measurement noise in the calibration, geometric errors, and errors due to diffraction. The random errors can be reduced by averaging multiple random ball tests. The geometric errors and diffraction errors are systematic, and arise when the radius of the CaliBall is different from that of the test optic.

Keywords: Random ball test, interferometer calibration, diffraction, retrace, imaging distortion

1. INTRODUCTION

For interferometric measurement of precision surfaces and wavefronts, errors from the reference surface and the surface under test are often the same order of magnitude. To achieve a measurement accuracy better than the reference surface, errors from the reference surface must be characterized and subtracted from the measurement result. These procedures are also called absolute tests. Over the years, a variety of calibration methods, such as the three-flat test[1], the three-position test[2] etc., have been developed for calibrating transmission spheres or flats.

The random ball test (RBT) has recently become a popular technique for calibrating spherical wavefronts [3]. In this test, a high-quality ball is measured against the reference surface at its confocal position in a number of random orientations shown in Fig. 1 (a), which averages out the errors due to the irregularity of the ball surface and converges toward the stationary error in the reference sphere. Practical experience with RBTs indicates that the number of ball orientations required for the calibration good to 1 nm rms is about 10 to 15[4], [5]. To maintain alignment while rotating the ball, the ball can be set on a kinematic support consisting of three smaller balls arranged in an equilateral triangle shown in Fig. 1 (b)[6]. The RBT is quite simple, easy to perform and does not require additional optics to perform the calibration.

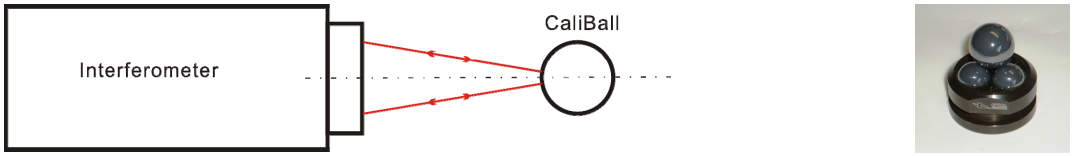

(a) (b)

Fig. 1. The random ball test. (a) The ball is measured at the confocal position. (b) The kinematic support for the ball.

However, the RBT has some remaining errors that limit the calibration. This paper details the three sources of errors of RBT. They are random error, geometric error and error due to diffraction.

2. ERRORS IN THE RANDOM BALL TEST

Errors are either random or systematic. Effects of random errors can be reduced by averaging many measurements. Systematic errors cannot be averaged out and will be left in the measurement if not calibrated. Geometric errors and errors due to diffraction are systematic, and are related to the test geometry. In the following sections, an example of using a 25 mm diameter CaliBall to calibrate a 6" F/3.2 transmission sphere on a Wyko interferometer is provided to estimate these three error sources.

2.1 Random error

Interferometric measurements suffer from noise, or random non-repeatability from one measurement to the next. The reason for this can be from the laser source instability, mechanical vibrations, air turbulence, detector noise, and so on. Averaging many measurements reduces the random noise in the test and improves the measurement accuracy. Fig. 2 shows an average of 34 random tests $\overline{W}$. This map will be used as a calibration map and subtracted from the surface measurement.

Optical Manufacturing and Testing VIII, edited by James H. Burge, Oliver W. Fähnle, Ray Williamson,
Proc. of SPIE Vol. 7426, 74260U · © 2009 SPIE · CCC code: 0277-786X/09/$18 · doi: 10.1117/12.828503

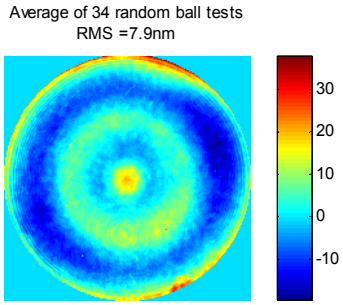

Fig. 2. An average of 34 random tests. A 25 mm CaliBall is used to calibrate a Wyko interferometer with a 6" F/3.2 transmission sphere

The variation in the data sets can be used to estimate the error in the individual maps and the magnitude of the residual error in a map created by an average of multiple measurements [4], [7]. From the 34 measurements, N maps (N = 1,3,5,7,9…) are chosen at random and averaged. This average map $\overline{W}_N$ is subtracted from $\overline{W}$, and the RMS value is calculated. This process is repeated several times, and the mean and the standard deviation of these RMS values are calculated. This is repeated for N from 1 to 19, and the results are plotted in both normal scale and log-log scale shown in Fig. 3. The curve follows the mean, and the error bar represents the standard deviation. In the log-log plot, the fitted straight line has a slope of -0.5, which means that the errors are random since it is dropping off as $1/\sqrt{N}$. It can be extrapolated that the error in the average of 34 random tests is 0.5 nm rms.

A plot like Fig. 3 is useful because it can be used to estimate the residual error in an average map and the number of measurements needed to achieve the desired accuracy. As measurement conditions improve, the slope of the log-log plot remains close to 0.5, but the entire curve shifts down.

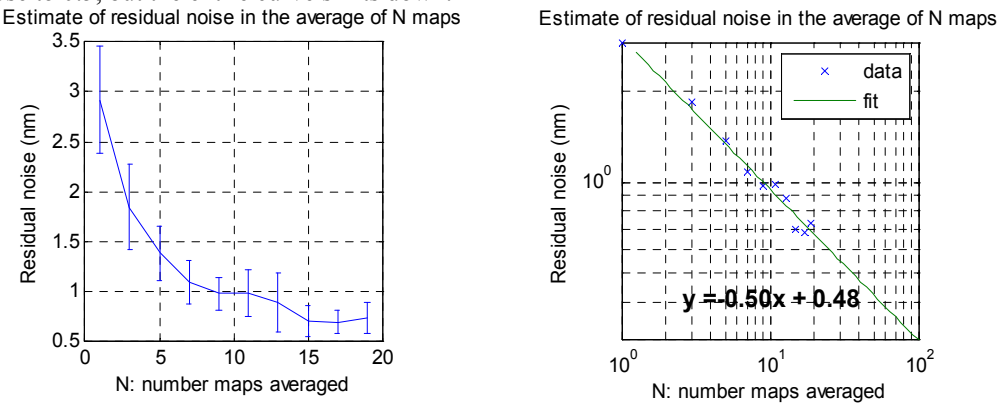

Fig. 3. The estimate of residual error in the average of N maps. (a) normal scale, (b) log-log scale.

2.2 Geometric effect

Geometric errors are intrinsic to the interferometer, including retrace error and imaging distortion. Retrace errors arise when the test and reference wavefronts mismatch, because, strictly speaking, they no longer share the common path. A special case of retrace errors is that the measured wavefront changes with different amounts of tilt added in the test [8]. Imaging distortion, which is non-linear mapping from the test optic to the interferogram, occurs especially when using a fast transmission sphere or null optics. It causes the surface defects to appear shifted and also causes the low order alignment errors to appear as high order wavefront errors [9].

These two errors can be compensated if the interferometer is completely characterized [10]. Unfortunately, it is difficult to completely characterize the interferometer without knowing the distances and optics properties inside. However, the first-order geometric errors are proportional to the wavefront slope and can be estimated using sensitivity functions by

$$\Delta W_{geo} = S_x(x,y)\nabla_x M + S_y(x,y)\nabla_y M \,, \qquad (1)$$

where M is the surface measurement and $\nabla_x M$ and $\nabla_y M$ are the slopes of the measurement in the x and y directions. S_x and S_y are the sensitivity functions to the x slope and y slope respectively, which are defined as linear combinations of Zernike polynomials

$$S_x(x,y) = \sum_i C_{xi} \cdot Z_i(x,y), \quad S_y(x,y) = \sum_i C_{yi} \cdot Z_i(x,y), \tag{2}$$

where C_i represents the coefficients of the corresponding Zernike polynomials $Z_i(x,y)$. The sensitivity functions have units of $\text{nm}/\mu\text{rad}$, and can be multiplied by the local slopes of a measurement to calculate the geometric errors. The procedure to find the geometric errors is:

1. Set up the interferometer, align the part to achieve minimum fringes (or null measurement), and take a measurement denoted as M. Also at every pixel, find the measurement local slope in the x and y directions denoted as $\nabla_x M$ and $\nabla_y M$, which have units of μrad.
2. Introduce various amounts of tilt along both the x axis and y axis, and record the wavefront maps. Subtract tilt and power from each measurement in the software. Any change from the null test is attributed to geometric errors. Fit each map to the low order Zernike polynomials ($a_{5n}, a_{6n}, a_{7n}, a_{8n}, a_{9n} \ldots$, where the subscript indicates the n^{th} measurement), and this is the first fit.
3. Find the effect of tilting the part on the coefficients of the low order Zernike polynomials. The terms that vary linearly with tilt (e.g. a_i) are the induced first-order geometric error. Find the sensitivity coefficients C_{xi} and C_{yi} based on a linear fit to a_{in} with varying amounts of tilt, and this is the second fit.
4. Apply the sensitivity functions to the slope of the surface measurement M, and calculate the geometric errors.

The reason to use low order Zernike polynomials to find sensitivity coefficients is that they act as a low-pass filter and are less sensitive to the measurement noise. Following the procedure described above, the low order Zernike coefficients are plotted as a function of tilt for the RBTs shown in Fig. 4. The coma x varies linearly with tilt x and the coma y varies linearly with tilt y. The other terms are almost unchanged. The sensitivity coefficients for the x and y coma are both $0.24\ \text{nm}/\mu\text{rad}$. Keeping only the single coma term that changes with tilt linearly, the sensitivity functions become

$$S_x(x,y) = 0.24 \cdot Z_8(x,y), \quad S_y(x,y) = 0.24 \cdot Z_7(x,y), \tag{3}$$

where $Z_7(x,y) = \sqrt{8}\left(3y^3 + 3x^2 y - 2y\right)$ and $Z_8(x,y) = \sqrt{8}\left(3x^3 + 3xy^2 - 2x\right)$. The plots of sensitivity functions are given in Fig. 5. If adding some power in the RBT, the spherical aberration will be introduced and the amount of spherical aberration can be predicted using Eq. (1) for a given power.

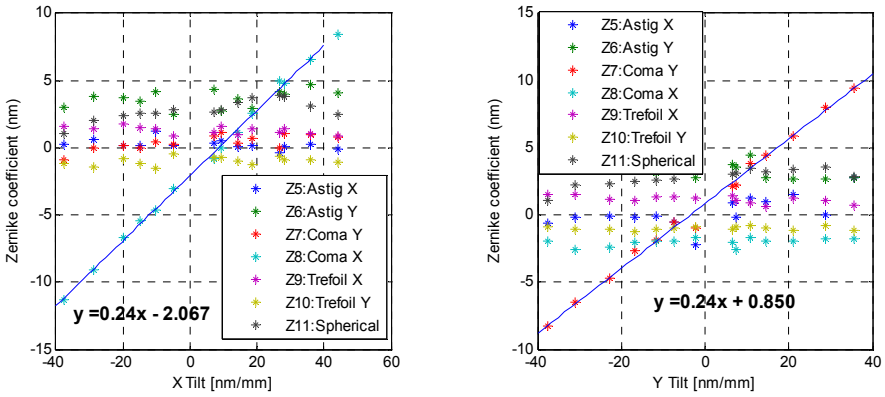

Fig. 4. Several lower-order Zernike coefficients are plotted as a function of x and y tilts to find the sensitivity coefficients.

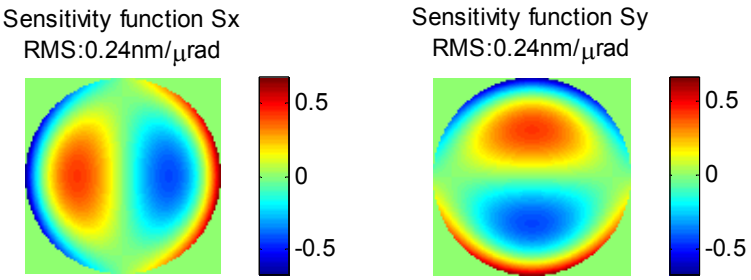

Fig. 5. The plots of the sensitivity functions S_x and S_y for the RBT

The measurement results due to different alignment errors in the RBT are shown in Fig. 6. Since the slope data is very sensitive to edge diffraction, small portion of data around the edge is clipped before this processing. Case (a) shows the data when the CaliBall was adjusted to have minimum fringes. Some tilt and power were introduced intentionally in case (b) and (c). The first column is the original data with tilt and power in the map, while the second column shows the data with tilt and power removed. From the second column, we can see that the measurements suffer from the geometric errors and they change with alignment errors. The next two columns show the maps of Slope X and Y, which are calculated based on the original data (the first column). The estimated geometric errors are given in the fifth column, which are subtracted from the original data and then removing tilt/power gives the compensated map shown in the last column. The compensated maps show that the geometric errors can be removed from the measurement using the sensitivity functions. The geometric error in the null test (case a) is mainly due to the local slope on the surface, and is about 0.7 nm rms.

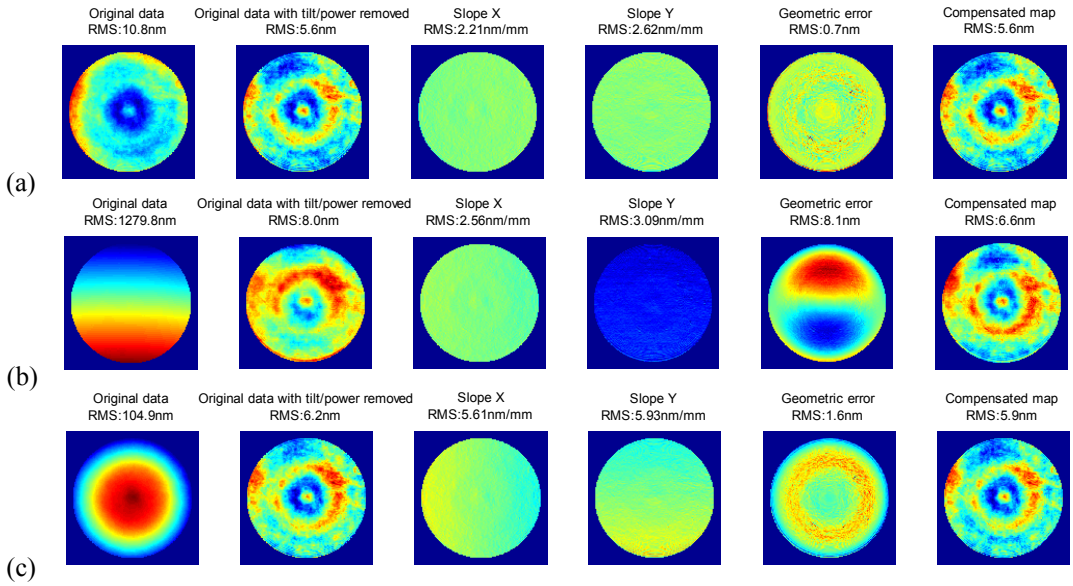

Fig. 6. Geometric errors when there are alignment errors. (a) Test with null fringe; (b) Test with -2.25λ of y tilt; (c) Test with -0.2λ of power. The coefficients for tilt and power are calculated using Zernike Standard Polynomials

2.3 Errors due to diffraction

In addition to geometric errors, the RBT also suffers errors due to wave propagation. It is best to perform the RBT after testing the surface of interest without changing the zoom or focus. This is because when the interferometer is used to test an optic, the imaging focus or zoom will be adjusted accordingly so that the interferometer images the test optic on the detector. The RBT can be performed afterwards without changing anything inside the interferometer. There are two tests, one is the RBT and the other is the test having the information of the surface of interest. To distinguish between them, the later one is called the surface measurement. Errors due to diffraction can be discussed from two aspects: phase smoothing and edge diffraction.

2.3.1 Phase smoothing

Diffraction effects cause a change in high spatial frequency components, which we call phase smoothing. Phase smoothing can be studied using the Talbot imaging theory [11], [12], and a brief explanation about using the Talbot imaging to calculate errors due to diffraction is provided in the Appendix. Phase smoothing can be discussed in three aspects: diffraction effects from the test wavefront, the reference wavefront, and the common wavefront.

Diffraction effects from the test wavefront

In the surface measurement, the diffraction effects from the test surface are avoided because the surface is focused onto the detector. In the RBT, the CaliBall is not in focus unless it has the same radius of curvature as the test surface. However, the CaliBall is rotated to many orientations and the average of all the measurements can be regarded as a perfect spherical surface. Therefore, one can assume there is no diffraction error from the CaliBall surface either.

Diffraction effects from the reference wavefront

In both the RBT and the surface measurement, the reference wavefronts are the same since no optics inside the interferometer are changed. The diffraction effects on the reference wavefronts in both tests can be cancelled, even though the reference surface may not be in focus.

Diffraction effects from the common wavefront

The common wavefront refers to the wavefront from the illumination optics in an interferometer. After passing through the beamsplitter inside an interferometer, the common wavefront splits into two beams, one in the reference arm and the other in the test arm. In both the RBT and the surface measurement, the common wavefront behaves the same in the reference beam, while it usually propagates different distances in the test beams as shown in Fig. 7. When the test surface has the same radius of curvature as the CaliBall, the common wavefront propagates the same distance in the two tests and will not introduce any errors due to diffraction effects.

Different propagation distances cause different phase smoothing of the common wavefront, and introduce errors. A transfer function, which is defined in the Appendix, predicts the filtering of high frequency phase ripples as the wavefront propagates from the transmission sphere to the test optic. If the wavefront at the transmission sphere is known, its phase attenuation as it propagates to the test optic (plane of focus) can be evaluated. In the RBT, it is a little complicated because there is a CaliBall in between. We can first find the conjugate plane of the wavefront at the transmission through the CaliBall's imaging, and then propagate that wavefront to the test optic. At the wavefront's conjugate plane, the phase ripple remains its complex amplitude. Our future paper will provide the equations for calculating the transfer functions for the surface measurement and the RBT [13]. Figure 8-11 list some calculation results for different radii of curvature of the test surface, different CaliBall sizes and transmission spheres.

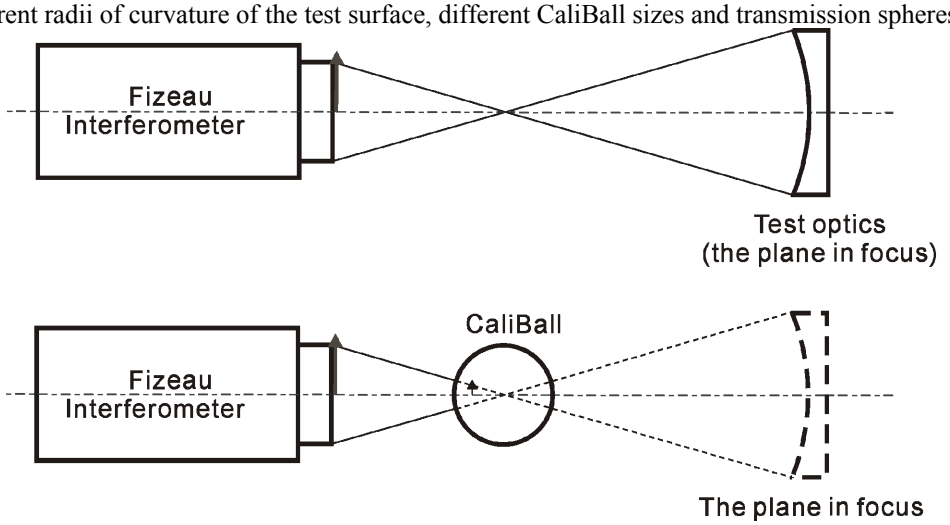

Fig. 7. Propagation of the common wavefront in the surface measurement (top) and in the RBT (bottom). The arrows represent the common wavefront and its conjugate through the CaliBall imaging.

Fig. 8 shows the transfer functions of the common wavefront as it propagates from the transmission sphere to the test optic (plane of focus) in the surface measurement and the RBT. The six lines in each plot represent the radii of the test surface from 100 mm to -1000 mm, respectively. The negative sign means the test surface is concave and a positive number means a convex surface. The smoothing of the common wavefront in the surface measurement is small when the radius of curvature of the test surface is large for both concave and convex surfaces. The RBT generally suffers from phase smoothing more than the surface measurement.

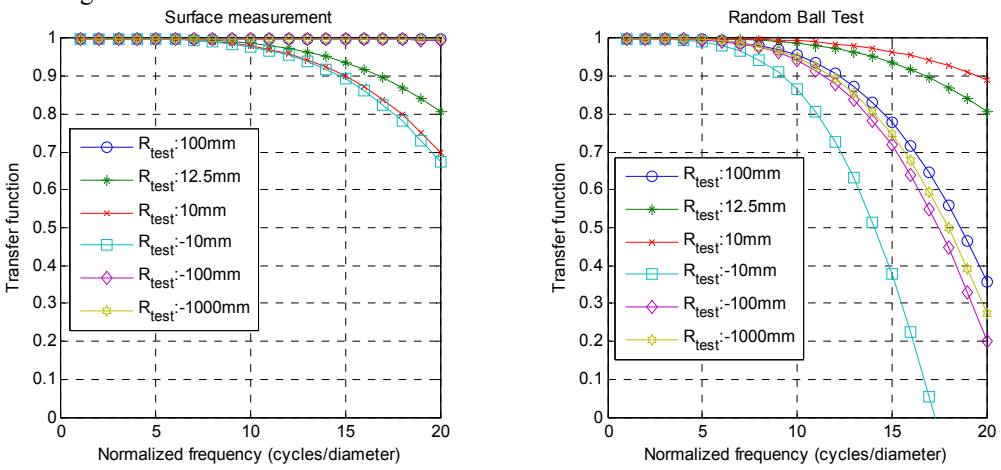

(a) (b)

Fig. 8. Transfer functions vs. spatial frequencies in (a) the surface measurement, (b) the RBT test. A 25 mm CaliBall is used to calibrate an F/3.2 transmission sphere with a beam diameter of 150 mm. The test optic has a radius of curvature of 100mm, 12.5mm (same as CaliBall radius), 10mm, -10mm, -100mm and -1000 mm respectively.

A sensitivity function, defined as the difference between the transfer functions of the surface measurement and the RBT, gives the measurement error due to the diffraction effect as a function of spatial frequency of the common wavefront, when using the RBT to calibrate the interferometer. Fig. 9 gives this sensitivity function which is the difference between Fig. 8(a) and Fig. 8(b), and it shows that the measurement errors due to diffraction are small when the phase ripples are less than 10 cycles/diameter. Note that for concave test surface, the change in sensitivity function decreases dramatically as the radius of the test surface becomes larger. For a convex surface, the errors due to phase smoothing cancelled out when the test optic has the same radius of curvature as the CaliBall. At the spatial frequency of 20 cycles/diameter, the sensitivity function versus the radius of curvature of the test surface is plotted in Fig. 10. It shows that as the radius of curvature increases for both concave and convex surfaces, the sensitivity function is approaching to an asymptote.

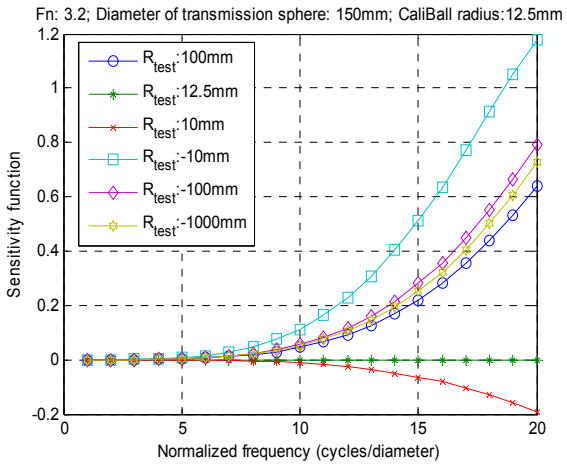

Fig. 9. The sensitivity function, defined as the difference between Fig. 8(a) and Fig. 8(b), gives the measurement error due to the diffraction effect as a function of the spatial frequency of the common wavefront, when using the RBT to calibrate the interferometer.

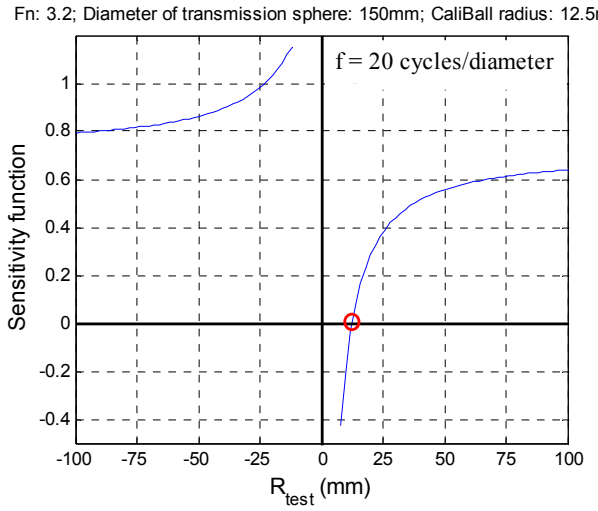

Fig. 10. The sensitivity functions versus the radius of curvature of the test surface at the spatial frequency of 20 cycles/diameter.

To investigate the effect of F-number and CaliBall size on the phase attenuation, we assume that the test optic is concave with a radius of curvature of 1000 mm and the diameter of the transmission sphere is 150 mm. Fig. 11 gives the sensitivity function at different F-numbers of the transmission sphere, and it shows that faster transmission spheres are less susceptible to error from the common wavefront.

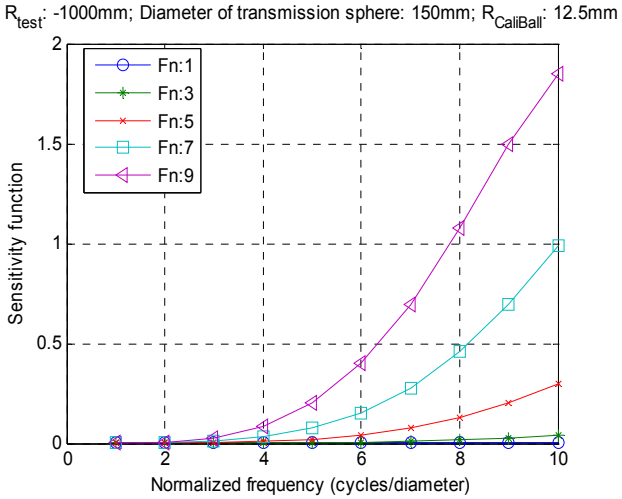

Fig. 11. The sensitivity function vs. spatial frequencies at different F numbers. The fast transmission spheres are less susceptible to error from the common wavefront.

The sensitivity function versus spatial frequency with different CaliBall sizes is plotted in Fig. 12. The F-number is 3.2 for all the three curves. It shows that larger CaliBall generally introduce less error, so it is better to choose larger diameter CaliBall for calibration if the CaliBall's radius of curvature cannot match that of the test surface.

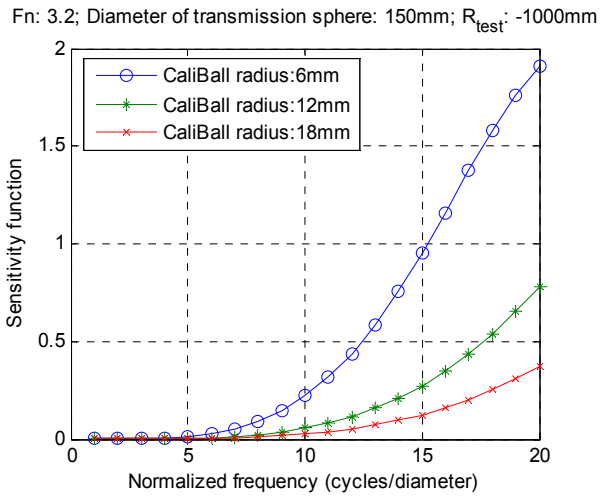

Fig. 12. The sensitivity function vs. spatial frequencies with different CaliBall size. The larger CaliBall generally introduce less error due to diffraction.

The diffraction errors from the common wavefront depend on the radii of curvature of the test surface and the CaliBall, and the F-number of the transmission sphere. In general, it is true that

- A concave test optic with a larger radius of curvature will have less error introduced from the common wavefront; a convex test optic with the same radius of curvature as the CaliBall will have no errors due to diffraction.
- A faster system will have less error from the common wavefront.
- A larger diameter CaliBall has smaller wavefront errors when the radius of curvature of the test surface is much larger than that of the CaliBall.

Phase smoothing only becomes noticeable when the phase ripple in the common wavefront has high spatial frequency. Usually, the wavefront coming out of an interferometer is of low spatial frequencies. Even if there are some high frequency contents, they are often small in magnitude. Therefore, errors due to phase smoothing are usually small.

Assume that there are 10 nm rms errors at 8 cycles/diameter in the common wavefront, the diameter of the transmission sphere is 6 inches, and the radius of curvature of the test optic is concave and much larger than the CaliBall size. The measurement errors due to phase smoothing at different F-numbers and CaliBall sizes are shown in Fig. 13. In the case of F/4 and 12 mm radius CaliBall, the RMS error due to phase smoothing is about 0.5 nm.

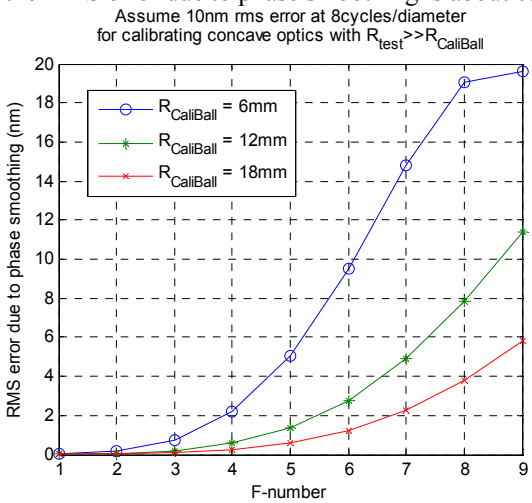

Fig. 13. The measurement error due to phase smoothing at various F-number and CaliBall size. Assume there are 10 nm rms errors at 8 cyles/diameter in the common wavefront, the diameter of the transmission sphere is 6 inches, and the radius of curvature of the test optic is concave and much larger than the CaliBall size.

2.3.2 Edge diffraction

Edge diffraction is seen when the aperture is not in focus. There are many apertures inside interferometers that cannot be in focus since interferometers often image the surface under test on the detector to correctly represent the errors in the test surface. However, edge diffraction from the limiting aperture usually has the most dominant effect in a measurement. In RBTs, one can often see the diffraction rings around the edge that is caused by the diffraction of the aperture of the transmission sphere. To simulate this edge diffraction, the aperture of the transmission sphere is imaged through the CaliBall at a position inside the CaliBall, then the diffraction pattern is calculated as a spherical wavefront propagating from that position to the test optic (plane of focus). We simulated this edge diffraction for the 6" F/3.2 and F/7 transmission spheres in MATLAB, for the case that the interferometer focuses at the test optic which is concave and has a radius of curvature of 1000 mm. The results are as shown in Fig. 14. Similar to phase smoothing, the slower transmission sphere has a larger RMS error due to edge diffraction.

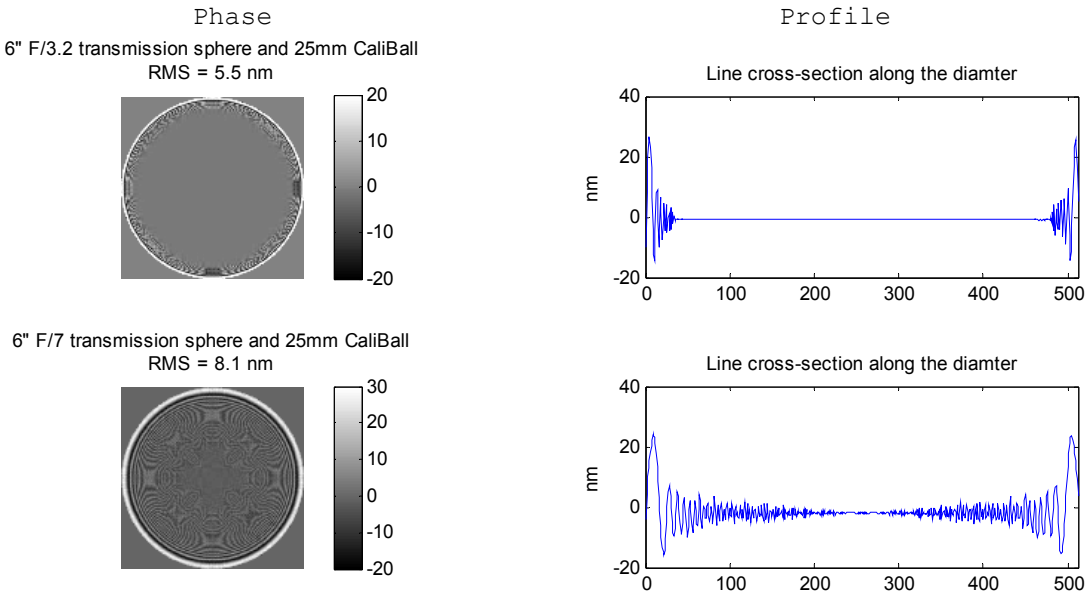

Fig. 14. Phase pattern due to edge diffraction (left) for the 6" F/3.2 and F/7 transmission spheres and their line profile (right).

If the test optic is overfilled by the beam coming out of interferometer, then only the corresponding portion of the calibration map and the edge diffraction are used. Assume that the test optic uses the central 80% of the clear aperture of the interferometer, the RMS errors due to edge diffraction at various F-numbers and CaliBall sizes are given in Fig. 15. With an F/3.2 transmission sphere and a 25 mm CaliBall, the error from edge diffraction is about 0.2 nm rms.

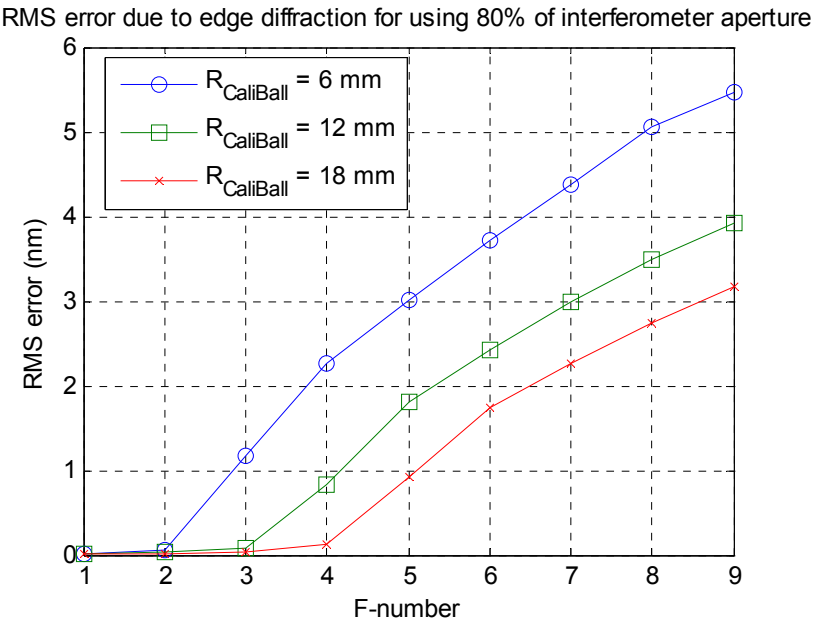

Fig. 15. RMS error due edge diffraction for using 80% of interferometer aperture. The diameter of transmission sphere is 6".

3. EXAMPLE

The total measurement uncertainty for the surface under test should include the measurement noise, geometric errors and the diffraction errors in both the random ball test and the surface measurement. If a 25 mm CaliBall is used to calibrate a 6" F/3.2 transmission sphere and the test part has a radius of curvature of 1000 mm, a reasonable breakdown of all these errors is listed in Table 1. Errors in the RBT are given based on the experimental data. Errors in the surface measurement depend on the part itself and the measurement environment. Here 1 nm of measurement noise is assigned to the surface measurement. If the sensitivity functions of the RBT and the surface measurement are the same and the test surface has the similar slope errors, the geometric error in the surface measurement will be similar to that of the RBT. The same amount of geometric error is assigned to the surface measurement. Note that the sensitivity function of the surface measurement usually is different from that of the RBT. If the common wavefront has 10 nm rms error at 8 cycle/diameter, then the errors due to phase smoothing is about 0.2 nm rms. The error due to edge diffraction is 0.2 nm rms within 80% of the aperture. Given the error budget shown in Table 1, the total measurement uncertainty is 1.5 nm rms.

Table 1. The total measurement uncertainty for the surface under test if the interferometer is calibrated with CaliBall

	Error sources	**Error budget**
Random Ball Test	Measurement noise	0.5 nm rms
	Geometric error	0.7 nm rms
Surface Measurement	Measurement noise	1 nm rms
	Geometric error	0.7 nm rms
Diffraction Effect	Phase smoothing	0.2 nm rms
	Edge diffraction (80% aperture)	0.2 nm rms
RSS error		1.5 nm rms

4. CONCLUSION

This paper extensively discusses the random and systematic errors using the random ball test, and provides the tools to quantify these errors. These tools can also be used to study the errors in other interferometric measurements. The RBT can calibrate the low spatial frequency errors to a good accuracy by averaging enough measurements. Some errors cannot be calibrated by the RBT when the radius of curvature of the test optic is different from the CaliBall radius.

The geometric errors are sensitive to the wavefront slope, while the diffraction effect becomes important for high spatial frequency contents and it comes in strongly for a slow transmission sphere and a small CaliBall. An example of estimating the remaining errors after interferometer calibration using the RBT is given and it shows that the total error is about 1.5 nm rms.

Appendix: Calculation of phase smoothing using Talbot imaging theory and effective propagation distance

Talbot imaging [12]:

Talbot imaging is a diffraction phenomenon that occurs for any wavefront with a periodic complex amplitude. If a wavefront with complex amplitude of a period of p is illuminated by collimated light, then that same complex amplitude is formed by free space diffraction at integer multiples of the Talbot distance $z_T = \frac{2p^2}{\lambda}$. As a sinusoidal phase pattern propagates, it will cycle through a reverse contrast amplitude pattern, a conjugate phase pattern, a pure amplitude pattern, then back to the original phase pattern.

If a wavefront with small phase ripples of W ($W << 1$) waves propagates a distance of L, then the magnitude of the ripples will be attenuated to [11]

$$W' = W\cos\left(2\pi\frac{L}{z_T}\right) = W\cos\left(\frac{\pi L\lambda}{p^2}\right). \qquad \text{(A1)}$$

Effective propagation distance:

The Talbot distance z_T is defined for a collimated beam. A converging wavefront starting with radius of curvature R_1, diameter $2a_1$, and ripples with period p_1, propagates to the position where it has a radius of curvature R_2, a beam diameter $2a_1\frac{R_2}{R_1}$, and ripples with a period $p_1\frac{R_2}{R_1}$ as shown in the figure below. To convert this propagation to equivalent propagation in collimated space, we evaluate the case where a lens with an arbitrary focal length f is used to convert the light into collimated light. Then we use geometric imaging relationships to calculate equivalent dimensions.

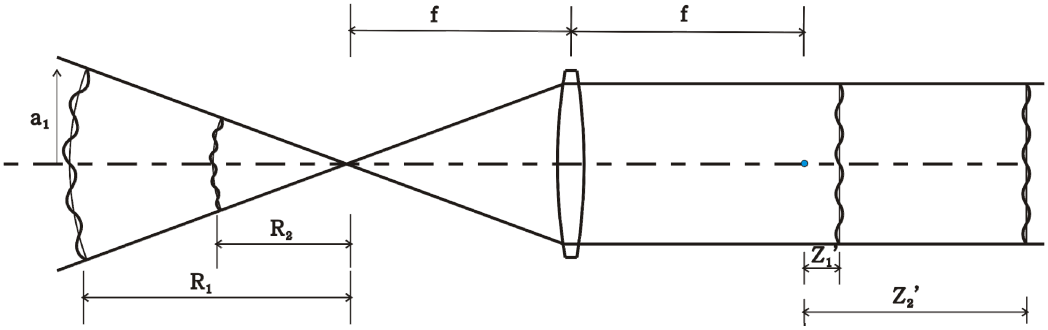

Fig. A1. Propagation in converging space is converted to equivalent propagation in collimated space.

In the collimated space, the equivalent propagation distance is

$$\Delta Z' = Z_2' - Z_1' = f^2\left(\frac{1}{R_2} - \frac{1}{R_1}\right), \qquad \text{(A2)}$$

and the phase ripple has a period of

$$p' = \frac{f}{R_1}p_1. \qquad \text{(A3)}$$

The attenuation of the phase ripple in the equivalent collimated space becomes

$$W' = W \cdot \cos\left(\frac{\pi\lambda \cdot \Delta Z'}{p'^2}\right) = W \cdot \cos\left(\frac{\pi\lambda R_1 \cdot (R_1 - R_2)}{R_2 \cdot p_1^2}\right) \quad . \tag{A4}$$

Comparing Eq. (A4) with Eq. (A1), it shows that $\frac{R_1(R_1 - R_2)}{R_2}$ is equivalent to L. Therefore, the effective propagation distance L_e can be defined as

$$L_e = \frac{R_1(R_1 - R_2)}{R_2}, \tag{A5}$$

and Eq. (A1) can be written as

$$W' = W \cdot \cos\left(\frac{\pi\lambda \cdot L_e}{p_1^2}\right) \quad . \tag{A6}$$

The period of the phase ripple p_1 can be normalized by the diameter $2a_1$, and then the normalized frequency $\frac{2a_1}{p_1}$ has a unit of cycles/diameter and it remains the same as it propagates. By replacing the period p_1 with the normalized frequency $f_{\text{normalized}}$, Eq. (A6) becomes

$$W' = W \cdot \cos\left(\frac{\pi\lambda \cdot L_e f^2_{\text{normalized}}}{4a_1^2}\right) \quad . \tag{A7}$$

A transfer function describing the magnitude of the wavefront smoothing, can be defined as

$$TF = \cos\left(\frac{\pi\lambda \cdot L_e}{p_1^2}\right) = \cos\left(\frac{\pi\lambda \cdot L_e f^2_{\text{normalized}}}{4a_1^2}\right). \tag{A8}$$

REFERENCES

[1] Schulz, G and Schwider, J., "Interferometric testing of smooth surfaces," in Progress in Optics (North-Holland, Amsterdam), Vol.13, 93-167 (1976).

[2] Jensen, A.E, "Absolute calibration method for Twyman-Green wavefront testing interferometer," J. Opt. Soc.Am. 63, 1313A (1973).

[3] Parks, R. E., Evans, C. J. and L. Shao, "Calibration of interferometer transmission spheres," in Optical Fabrication and Testing Workshop OSA Technical Digest Series 12, 80-83 (1998).

[4] Griesmann, U., Wang, Q., Soons, J., and Carakos, R., "A simple ball averager for reference sphere calibrations," Proc. SPIE 5869, 58690S-1 – 58690S-8 (2005).

[5] Burke, J., Green, K., Stuart, W., Puhanic, E., Leistner, A. and Oreb, B., "Fabrication and testing of a high-precision concave spherical mirror,", Proc. SPIE 7064, 7064E-1 – 7064E-10 (2008)

[6] Parks, R. E., "A Practical Implementation of the Random Ball Test," in Frontiers in Optics, OSA Technical Digest (CD) (Optical Society of America, 2006), paper OFMC12.

[7] Zhou, P., and Burge, J. H., "Calibration limits for interferometric measurements," OSA/OF&T, OWA3 (2008).

[8] Evans, C. J., "Compensation for errors introduced by nonzero fringe densities in phase-measuing interferometers," CIRP Annals 42/1, 577-580 (1993)

[9] Selberg, L. A., "Interferometer accuracy and precision," Proc. SPIE 1400, 24-32, (1990).

[10] Murphy, P. E., Brown, T.G. and Moore, D. T., "Measurement and calibration of interferometric imaging aberrations,",Appied Optics Vol.39, No.34, 6421-6429 (2000).

[11] Zhao, C. and Burge, J., "Imaging aberrations from null correctors," Proc. SPIE 6723, 67230L-1—67230L-12 (2007).

[12] Goodman, J., [Introduction to Fourier Optics], Roberts and Company Publisher, 88-91 (2005).

[13] Zhou, P. and Burge, J. H., "Analysis of diffraction effects for interferometric measurement", to be submitted to Applied Optics.